### Title
Artificial magnetism at terahertz frequencies from three-dimensional lattices of TiO_2 microspheres accounting for spatial dispersion and magnetoelectric coupling




### Journal
Journal of the Optical Society of America B, 31(5)

### ISSN
0740-3224



### Authors
Lannebère, Sylvain
Campione, Salvatore
Aradian, Ashod
et al.



### Publication Date
2014-05-01

### DOI
10.1364/josab.31.001078

Peer reviewed

# Artificial magnetism at terahertz frequencies from three-dimensional lattices of $TiO_2$ microspheres accounting for spatial dispersion and magnetoelectric coupling

**Sylvain Lannebère,[1,*] Salvatore Campione,[2] Ashod Aradian,[3] Matteo Albani,[4] and Filippo Capolino[2]**

[1]*Department of Information Engineering, University of Siena, 53100 Siena, Italy*
[2]*Department of Electrical Engineering and Computer Science, University of California, Irvine, California 92697, USA*
[3]*Centre de Recherche Paul Pascal (CRPP), CNRS-University of Bordeaux, 115 Av. Schweitzer, 33600 PESSAC, France*
[4]*Department of Information Engineering, University of Siena, 53100 Siena, Italy*
**Corresponding author: sylvain.lannebere@gmail.com*

Received March 13, 2014; accepted March 13, 2014;
posted March 12, 2014 (Doc. ID 200698); published April 11, 2014

We employ the generalized Lorentz–Lorenz method to investigate how both magnetoelectric coupling and spatial dispersion influence the artificial magnetic capabilities at terahertz frequencies of the representative case of a metamaterial consisting of a three-dimensional (3D) lattice of $TiO_2$ microspheres. The complex wavenumber dispersion relations pertaining to modes supported by the array, traveling along one of the principal axes of the array with electric or magnetic field polarized transversely and longitudinally (with respect to the mode traveling direction), are studied and thoroughly characterized. One mode with transverse polarization is dominant at any given frequency for the analyzed dimensions, proving that the 3D lattice can be treated as a homogeneous medium with defined electromagnetic material parameters. We show, however, that bianisotropy is a direct consequence of magnetoelectric coupling, and the dyadic expressions of both *effective* and *equivalent* material parameters are derived. In particular, we analyze the effect of spatial dispersion on the effective parameters relative to a composite material made by a 3D lattice of $TiO_2$ microspheres with filling fraction around 30% and near the first Mie magnetic dipolar resonance. Finally, we homogenize the metamaterial in terms of equivalent index and impedance, and by comparison with full-wave simulations, we explain the presence of the unphysical antiresonance permittivity behavior observed in previous work. 

*OCIS codes:* (160.3918) Metamaterials; (160.1245) Artificially engineered materials; (260.2065) Effective medium theory.
http://dx.doi.org/10.1364/JOSAB.31.001078

## 1. INTRODUCTION

Macroscopic field Maxwell equations must be supplemented by constitutive relations that model the electromagnetic properties of a given medium [1–3]. The introduction of *effective* electromagnetic parameters of a material describing a heterogeneous structure is called *homogenization* and has attracted a great deal of attention. Homogenization leads to the prediction of macroscopic effective dielectric properties of the mixture, depending on the parameters characterizing the heterostructure, such as the constituent permittivities and their fractional volumes. Simple theories, for example, the ones employing quasi-static approximation [4,5], do not deal with electromagnetic coupling and spatial dispersion, and as such may not be sufficient to describe the complex behavior of metamaterials, artificial materials with nonconventional or exotic electromagnetic response. Recently, more refined homogenization theories [6–14] have been developed to take into account complex effects, such as chirality, spatial dispersion, and/or magnetoelectric coupling.

Metamaterials made of nonmagnetic dielectric microspheres with large permittivity embedded in a host medium were studied in the gigahertz [15,16] and infrared frequency ranges [17,18]. Such metamaterials exhibit very strong magnetic response due to the presence of a strong Mie magnetic dipolar resonance of the dielectric spheres. We note that large losses are detrimental and indeed limit the artificial magnetic performance. For example, ceramic materials like the one used in [19] are not suitable materials at terahertz frequencies because they present large losses there, although they are convenient at microwave frequencies, where they exhibit large permittivity values with low losses. Among all potential high-permittivity materials at terahertz frequencies, $TiO_2$ (in rutile crystalline form as shown in Fig. 1) is in our opinion the best candidate [20] with a permittivity around 100 [21,22]. We have indeed shown in [23], with the help of extended Maxwell–Garnett theory, single dipole approximation [24], and full-wave simulations that three-dimensional (3D) lattices of $TiO_2$ microspheres give rise to strong magnetic response similar to that observed, for example, in [15–18].

We focus here on the generalized Lorentz–Lorenz method reported in [6], based on the Floquet representation, to homogenize a 3D lattice of $TiO_2$ microspheres at terahertz frequencies. Our aim is to thoroughly analyze the magnetic properties of this 3D lattice and show how these are affected by magnetoelectric effects. Similar properties are, however, expected from other 3D structures made of resonators with

 

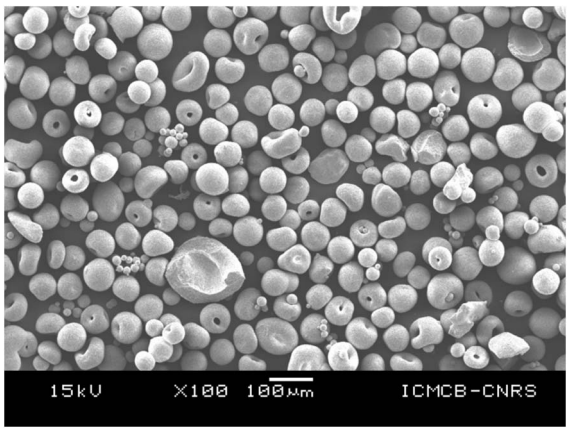


Fig. 1. $TiO_2$ (rutile) microspheres with a diameter around 70 µm provided by Dr. Chung-Seu, CNRS, Univ. Bordeaux, ICMCB, UPR 9048, F-33600 Pessac, France.

different shapes and materials also in other frequency ranges, provided each resonator exhibits a strong Mie dipolar magnetic resonance. As a step further in the understanding of these systems, we also analyze the dependence of the effective parameters on the wavevector, generally referred to as nonlocality or spatial dispersion.

This paper is organized as follows: in Section 2, we derive for the first time, to the authors' knowledge, the dyadic expressions for both the *effective* and the *equivalent* effective parameters (according to the nomenclature introduced in [11]) following the homogenization method reported in [6], accounting for magnetoelectric coupling. We confirm that when magnetoelectric coupling is not negligible the medium becomes bianisotropic. In addition, the method further allows for the computation of the eigenmodes with complex wavenumber supported by the array, helpful in the understanding of wave propagation within the 3D lattice. In Section 3, this formalism is eventually applied to a 3D lattice of $TiO_2$ microspheres. In particular, the modes with complex wavenumber propagating inside the structure are characterized, and the effects of spatial dispersion and magnetoelectric coupling on the effective parameters are emphasized. Moreover, comparisons with full-wave simulations are provided, showing excellent agreement of both artificial magnetism and scattering properties by using the equivalent parameters.

## 2. FORMULATION FOR THE TREATMENT OF 3D LATTICES ACCOUNTING FOR MAGNETOELECTRIC COUPLING AND SPATIAL DISPERSION

### A. Microsphere Modeling

We consider a 3D lattice of $TiO_2$ microspheres with radius $R$ and relative permittivity $\varepsilon_m^{\text{rel}} = 94 + 2.35\text{i}$ (corresponding to the permittivity of bulk $TiO_2$ at terahertz frequencies [21]) embedded into a host medium with absolute permittivity $\varepsilon_h$.

Each sphere will in general scatter a field that can be represented by a multipole series expansion. If the spheres' dimensions are sufficiently subwavelength, one can approximate the response of each sphere with dipolar terms only, in particular electric dipole $\mathbf{p}_e$ in [Cm] and magnetic dipole $\mathbf{p}_m$ in [Wbm], given by

$$\mathbf{p}_e = \varepsilon_h \alpha_{ee} \mathbf{E}_{\text{loc}}, \quad \mathbf{p}_m = \alpha_{mm} \mathbf{B}_{\text{loc}}, \tag{1}$$

where $\alpha_{ee}$ and $\alpha_{mm}$ (both in $[m^3]$) are the isotropic electric and magnetic polarizabilities of the microsphere, and $\mathbf{E}_{\text{loc}}$ and $\mathbf{B}_{\text{loc}}$ are the local electric field and the local magnetic flux density at the microsphere location. The dipolar approximation is a good approximation when the two dipolar terms (or any of them) dominate the scattered-field multipole expansion. The monochromatic time harmonic convention, $e^{-i\omega t}$, is implicitly assumed throughout the paper and thus suppressed hereafter. The dynamic Mie polarizabilities are [25]

$$\alpha_{ee} = 6\pi i a_1 \frac{1}{k_h^3}, \quad \alpha_{mm} = 6\pi i b_1 \frac{1}{k_h^3}. \tag{2}$$

These polarizabilities depend on the electric $a_1$ and magnetic $b_1$ Mie dipolar coefficients [26] given by

$$\begin{aligned} a_1 &= \frac{m\psi_1(mk_hR)\psi_1'(k_hR) - \psi_1(k_hR)\psi_1'(mk_hR)}{m\psi_1(mk_hR)\xi_1'(k_hR) - \xi_1(k_hR)\psi_1'(mk_hR)}, \\ b_1 &= \frac{\psi_1(mk_hR)\psi_1'(k_hR) - m\psi_1(k_hR)\psi_1'(mk_hR)}{\psi_1(mk_hR)\xi_1'(k_hR) - m\xi_1(k_hR)\psi_1'(mk_hR)}, \end{aligned} \tag{3}$$

where $\psi_1$, $\xi_1$ are the Riccati–Bessel functions [27], $k_h = \omega\sqrt{\varepsilon_h\mu_0} = k_0\sqrt{\varepsilon_h^{\text{rel}}}$ is the wavenumber inside the host medium, $m = \sqrt{\varepsilon_m^{\text{rel}}/\varepsilon_h^{\text{rel}}}$ is the relative refractive index contrast, and $\varepsilon_h^{\text{rel}}$ is the relative permittivity of the host medium. The $'$ in Eq. (3) denotes here the derivative with respect to the argument.

### B. Effective Medium Theory via Green's Function Method

We employ the model developed in [6] to compute the electromagnetic properties of a 3D lattice as in the left panel of Fig. 2 excited by an external electric current density

$$\mathbf{J}_e(\mathbf{r}) = \mathbf{J}_{e,\text{av}} e^{i\mathbf{k}\cdot\mathbf{r}}, \tag{4}$$

where $\mathbf{J}_{e,\text{av}}$ is an average current vector, $\mathbf{k}$ is an assigned wavevector, and $\mathbf{r}$ is the observation vector.

For the sake of simplicity, we keep the same notation used in [6]. The local electric field $\mathbf{E}_{\text{loc}}$ and magnetic flux density $\mathbf{B}_{\text{loc}}$ evaluated at $\mathbf{r} = \mathbf{0}$ (i.e., at the reference sphere location), given by Eq. (27) of [6], are

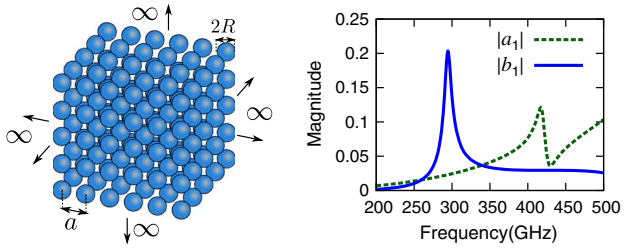


Fig. 2. On the left, schematic for a 3D periodic cubic array with lattice parameter $a$ composed of $TiO_2$ microspheres with radius $R$. On the right, frequency behavior of the magnitude of the dipolar Mie magnetic ($b_1$) and electric ($a_1$) coefficients given by Eq. (3), in free space for spheres of $TiO_2$ with radius $R = 52$ µm.

$$\mathbf{E}_{\mathrm{loc}} = \mathbf{E}_{\mathrm{av}} + \bar{\bar{\mathbf{C}}}_{\mathrm{int}}(\omega,\mathbf{k})\cdot\frac{\mathbf{p}_e}{\varepsilon_h} + \bar{\bar{\mathbf{C}}}_{\mathrm{em}}(\omega,\mathbf{k})\cdot\frac{\mathbf{p}_m}{\sqrt{\varepsilon_h\mu_0}},$$
$$\frac{\mathbf{B}_{\mathrm{loc}}}{\mu_0} = \mathbf{H}_{\mathrm{av}} - \bar{\bar{\mathbf{C}}}_{\mathrm{em}}(\omega,\mathbf{k})\cdot\frac{\mathbf{p}_e}{\sqrt{\mu_0\varepsilon_h}} + \bar{\bar{\mathbf{C}}}_{\mathrm{int}}(\omega,\mathbf{k})\cdot\frac{\mathbf{p}_m}{\mu_0}, \tag{5}$$

where $\mathbf{E}_{\mathrm{av}}$ and $\mathbf{H}_{\mathrm{av}}$ are the average macroscopic fields, and $\bar{\bar{\mathbf{C}}}_{\mathrm{int}}(\omega,\mathbf{k})$ is the so-called interaction dyadic (evaluated at $\mathbf{r}=\mathbf{0}$), defined by Eq. (14) of [6], that expresses the interaction between the reference microsphere and the field produced by the other microspheres in the array. In other words, the term $\bar{\bar{\mathbf{C}}}_{\mathrm{int}}(\omega,\mathbf{k})$ is the dyadic Green's function for the periodic array of dipoles regularized in both the space and spectral domains and is evaluated, for fast convergence, through the Ewald method [14,23,28–30]. Two bars on top of a bold letter indicate a dyadic quantity. The term $\bar{\bar{\mathbf{C}}}_{\mathrm{em}}(\omega,\mathbf{k})$ is the magnetoelectric coupling dyad, defined by Eq. (28) of [6], that describes the interaction between electric and magnetic dipoles in the array (we do not account for magnetoelectric coupling at the unit cell level that would rise only for nonsymmetrical resonators [31]).

By using the definition of the average macroscopic magnetic field

$$\mathbf{H}_{\mathrm{av}} = \frac{\mathbf{B}_{\mathrm{av}}}{\mu_0} - \frac{\mathbf{p}_m}{V_{\mathrm{cell}}\mu_0} \tag{6}$$

with $V_{\mathrm{cell}}$ the volume of the unit cell of the 3D lattice, together with the expression of the local fields (5) and the dipole information (1), we obtain the relation between the average fields and the microscopic dipoles

$$(\bar{\bar{\mathbf{I}}} - \alpha_{ee}\bar{\bar{\mathbf{C}}}_{\mathrm{int}}(\omega,\mathbf{k}))\cdot\frac{\mathbf{p}_e}{\varepsilon_h} - \alpha_{ee}\bar{\bar{\mathbf{C}}}_{\mathrm{em}}(\omega,\mathbf{k})\cdot\frac{\mathbf{p}_m}{\sqrt{\varepsilon_h\mu_0}} = \alpha_{ee}\mathbf{E}_{\mathrm{av}},$$
$$(\bar{\bar{\mathbf{I}}} - \alpha_{mm}\bar{\bar{\mathbf{C}}}_{\mathrm{int}}(\omega,\mathbf{k}))\cdot\frac{\mathbf{p}_m}{\mu_0} + \alpha_{mm}\bar{\bar{\mathbf{C}}}_{\mathrm{em}}(\omega,\mathbf{k})\cdot\frac{\mathbf{p}_e}{\sqrt{\mu_0\varepsilon_h}} = \alpha_{mm}\mathbf{H}_{\mathrm{av}}, \tag{7}$$

with $\bar{\bar{\mathbf{I}}}$ denoting the unit dyad.

### C. Dyadic Expressions for Effective Parameters

In the original paper [6], the term $\bar{\bar{\mathbf{C}}}_{\mathrm{em}}$ was neglected in the definition of the effective parameters. Our goal in this section is to derive the dyadic expressions of the effective parameters $\bar{\bar{\varepsilon}}_{\mathrm{eff}}$ and $\bar{\bar{\boldsymbol{\mu}}}_{\mathrm{eff}}$, accounting also for the magnetoelectric coupling term $\bar{\bar{\mathbf{C}}}_{\mathrm{em}}$. A similar analysis has been recently done in [11], where, however, the dyadic form for the effective parameters was not investigated.

The macroscopic average polarization and magnetization are defined by

$$\mathbf{P}_{\mathrm{av}} = \frac{\mathbf{p}_e}{V_{\mathrm{cell}}}, \qquad \mathbf{M}_{\mathrm{av}} = \frac{\mathbf{p}_m}{V_{\mathrm{cell}}\mu_0}, \tag{8}$$

and allow us to write Eq. (7) in block matrix form as

$$\begin{bmatrix}\mathbf{P}_{\mathrm{av}}\\ \mu_0\mathbf{M}_{\mathrm{av}}\end{bmatrix} = \begin{bmatrix}\varepsilon_h\bar{\bar{\boldsymbol{\chi}}}_{ee}(\omega,\mathbf{k}) & \sqrt{\varepsilon_h\mu_0}\bar{\bar{\boldsymbol{\chi}}}_{em}(\omega,\mathbf{k})\\ \sqrt{\varepsilon_h\mu_0}\bar{\bar{\boldsymbol{\chi}}}_{me}(\omega,\mathbf{k}) & \mu_0\bar{\bar{\boldsymbol{\chi}}}_{mm}(\omega,\mathbf{k})\end{bmatrix}\cdot\begin{bmatrix}\mathbf{E}_{\mathrm{av}}\\ \mathbf{H}_{\mathrm{av}}\end{bmatrix}. \tag{9}$$

The block matrix of susceptibilities $\bar{\bar{\boldsymbol{\chi}}}$ is given by

$$\begin{bmatrix}\bar{\bar{\boldsymbol{\chi}}}_{ee}(\omega,\mathbf{k}) & \bar{\bar{\boldsymbol{\chi}}}_{em}(\omega,\mathbf{k})\\ \bar{\bar{\boldsymbol{\chi}}}_{me}(\omega,\mathbf{k}) & \bar{\bar{\boldsymbol{\chi}}}_{mm}(\omega,\mathbf{k})\end{bmatrix} = \frac{1}{V_{\mathrm{cell}}}\begin{bmatrix}\bar{\bar{\mathbf{I}}} - \alpha_{ee}\bar{\bar{\mathbf{C}}}_{\mathrm{int}}(\omega,\mathbf{k}) & -\alpha_{ee}\bar{\bar{\mathbf{C}}}_{\mathrm{em}}(\omega,\mathbf{k})\\ \alpha_{mm}\bar{\bar{\mathbf{C}}}_{\mathrm{em}}(\omega,\mathbf{k}) & \bar{\bar{\mathbf{I}}} - \alpha_{mm}\bar{\bar{\mathbf{C}}}_{\mathrm{int}}(\omega,\mathbf{k})\end{bmatrix}^{-1}\cdot\begin{bmatrix}\alpha_{ee}\bar{\bar{\mathbf{I}}} & \bar{\bar{\mathbf{0}}}\\ \bar{\bar{\mathbf{0}}} & \alpha_{mm}\bar{\bar{\mathbf{I}}}\end{bmatrix}. \tag{10}$$

In Eq. (9), the macroscopic polarization $\mathbf{P}_{\mathrm{av}}$ and magnetization $\mathbf{M}_{\mathrm{av}}$ depend on both $\mathbf{E}_{\mathrm{av}}$ and $\mathbf{H}_{\mathrm{av}}$, and, consequently, the displacement field $\mathbf{D}_{\mathrm{av}} = \varepsilon_h\mathbf{E}_{\mathrm{av}} + \mathbf{P}_{\mathrm{av}}$ and the magnetic flux density $\mathbf{B}_{\mathrm{av}} = \mu_0(\mathbf{H}_{\mathrm{av}} + \mathbf{M}_{\mathrm{av}})$ depend also on both $\mathbf{E}_{\mathrm{av}}$ and $\mathbf{H}_{\mathrm{av}}$. In this condition, the medium is said to be bianisotropic [32,33] and the constitutive relations in this type of medium are

$$\mathbf{D}_{\mathrm{av}} = \bar{\bar{\varepsilon}}_{\mathrm{eff}}(\omega,\mathbf{k})\cdot\mathbf{E}_{\mathrm{av}} + \bar{\bar{\boldsymbol{\xi}}}_{\mathrm{eff}}(\omega,\mathbf{k})\cdot\mathbf{H}_{\mathrm{av}},$$
$$\mathbf{B}_{\mathrm{av}} = \bar{\bar{\boldsymbol{\mu}}}_{\mathrm{eff}}(\omega,\mathbf{k})\cdot\mathbf{H}_{\mathrm{av}} + \bar{\bar{\boldsymbol{\zeta}}}_{\mathrm{eff}}(\omega,\mathbf{k})\cdot\mathbf{E}_{\mathrm{av}}. \tag{11}$$

The electromagnetic properties of the material with this formulation are then described by the four dyadics

$$\bar{\bar{\varepsilon}}_{\mathrm{eff}}(\omega,\mathbf{k}) = \varepsilon_h(\bar{\bar{\mathbf{I}}} + \bar{\bar{\boldsymbol{\chi}}}_{ee}(\omega,\mathbf{k})), \qquad \bar{\bar{\boldsymbol{\xi}}}_{\mathrm{eff}}(\omega,\mathbf{k}) = \sqrt{\varepsilon_h\mu_0}\bar{\bar{\boldsymbol{\chi}}}_{em}(\omega,\mathbf{k}),$$
$$\bar{\bar{\boldsymbol{\zeta}}}_{\mathrm{eff}}(\omega,\mathbf{k}) = \sqrt{\varepsilon_h\mu_0}\bar{\bar{\boldsymbol{\chi}}}_{me}(\omega,\mathbf{k}), \qquad \bar{\bar{\boldsymbol{\mu}}}_{\mathrm{eff}}(\omega,\mathbf{k}) = \mu_0(\bar{\bar{\mathbf{I}}} + \bar{\bar{\boldsymbol{\chi}}}_{mm}(\omega,\mathbf{k})), \tag{12}$$

where the explicit expressions of the different susceptibility dyadics $\bar{\bar{\boldsymbol{\chi}}}$ are given by Eq. (10).

For example, it can be emphasized that when $\mathbf{k} = k\hat{\mathbf{x}}$, where the hat indicates a unit vector, the $yy$ and $zz$ components of the tensors in Eq. (12) correspond exactly to the effective parameters derived in Eq. (23) of [11] (e.g., using the notation in [11], looking at Eq. (22), the parameters $\bar{\bar{\boldsymbol{\xi}}}_{\mathrm{eff}}$ and $\bar{\bar{\boldsymbol{\xi}}}_{\mathrm{eff}}$ would be written as $\chi^o_{\mathrm{eff}}(\hat{\mathbf{k}}\times\bar{\bar{\mathbf{I}}})$ and $-\chi^o_{\mathrm{eff}}(\hat{\mathbf{k}}\times\bar{\bar{\mathbf{I}}})$, respectively, with $\hat{\mathbf{k}} = \mathbf{k}/k$).

### D. Modes Supported by the Metamaterial Array

In the previous section we have derived the effective material parameters for an arbitrary pair $(\omega,\mathbf{k})$, where $\omega$, $\mathbf{k}$ are independent of each other. However, in the absence of external excitation $\mathbf{J}_e$, only a discrete number of allowed pairs $(\omega,\mathbf{k})$ exists. Moreover, at a given radian frequency $\omega$ only a limited number of wavevectors are supported assuming low attenuation constant. These wavevectors correspond to the eigenmodes of the system described next and are of essential interest for the physical description of wave propagation.

In [34], it is demonstrated that by using the homogenized parameters into the homogeneous medium wave equation one can calculate the wavevector dispersion relation of the metamaterial.

The homogeneous wave equation is deduced from Maxwell equations with no sources together with the constitutive relation for the bianisotropic medium (11)

$$\mathbf{k}\times\mathbf{E}_{\mathrm{av}} = \omega\mathbf{B}_{\mathrm{av}} = \omega(\bar{\bar{\boldsymbol{\mu}}}_{\mathrm{eff}}(\omega,\mathbf{k})\cdot\mathbf{H}_{\mathrm{av}} + \bar{\bar{\boldsymbol{\xi}}}_{\mathrm{eff}}(\omega,\mathbf{k})\cdot\mathbf{E}_{\mathrm{av}}),$$
$$\mathbf{k}\times\mathbf{H}_{\mathrm{av}} = -\omega\mathbf{D}_{\mathrm{av}} = -\omega(\bar{\bar{\varepsilon}}_{\mathrm{eff}}(\omega,\mathbf{k})\cdot\mathbf{E}_{\mathrm{av}} + \bar{\bar{\boldsymbol{\xi}}}_{\mathrm{eff}}(\omega,\mathbf{k})\cdot\mathbf{H}_{\mathrm{av}}). \tag{13}$$

Equations (13) can be rearranged as

$$\mathbf{H}_{\mathrm{av}} = \bar{\bar{\boldsymbol{\mu}}}_{\mathrm{eff}}^{-1} \cdot \left( \frac{\mathbf{k}}{\omega} \times \bar{\bar{\mathbf{I}}} - \bar{\bar{\boldsymbol{\xi}}}_{\mathrm{eff}} \right) \cdot \mathbf{E}_{\mathrm{av}},$$
$$\mathbf{E}_{\mathrm{av}} = -\bar{\bar{\varepsilon}}_{\mathrm{eff}}^{-1} \cdot \left( \frac{\mathbf{k}}{\omega} \times \bar{\bar{\mathbf{I}}} + \bar{\bar{\boldsymbol{\xi}}}_{\mathrm{eff}} \right) \cdot \mathbf{H}_{\mathrm{av}}. \quad (14)$$

Combining the two equations in (14) we obtain the homogeneous wave equation in a matricial form for the electric field

$$\left[ \left( \frac{\mathbf{k}}{\omega} \times \bar{\bar{\mathbf{I}}} + \bar{\bar{\boldsymbol{\xi}}}_{\mathrm{eff}}(\omega, \mathbf{k}) \right) \cdot \bar{\bar{\boldsymbol{\mu}}}_{\mathrm{eff}}^{-1}(\omega, \mathbf{k}) \cdot \left( \frac{\mathbf{k}}{\omega} \times \bar{\bar{\mathbf{I}}} - \bar{\bar{\boldsymbol{\zeta}}}_{\mathrm{eff}}(\omega, \mathbf{k}) \right) + \bar{\bar{\varepsilon}}_{\mathrm{eff}}(\omega, \mathbf{k}) \right] \cdot \mathbf{E}_{\mathrm{av}} = \mathbf{0}, \quad (15)$$

and for the magnetic field

$$\left[ \left( \frac{\mathbf{k}}{\omega} \times \bar{\bar{\mathbf{I}}} - \bar{\bar{\boldsymbol{\zeta}}}_{\mathrm{eff}}(\omega, \mathbf{k}) \right) \cdot \bar{\bar{\varepsilon}}_{\mathrm{eff}}^{-1}(\omega, \mathbf{k}) \cdot \left( \frac{\mathbf{k}}{\omega} \times \bar{\bar{\mathbf{I}}} + \bar{\bar{\boldsymbol{\xi}}}_{\mathrm{eff}}(\omega, \mathbf{k}) \right) + \bar{\bar{\boldsymbol{\mu}}}_{\mathrm{eff}}(\omega, \mathbf{k}) \right] \cdot \mathbf{H}_{\mathrm{av}} = \mathbf{0}. \quad (16)$$

The solutions of these equations are found by imposing the determinant of the matrices to vanish. Solutions are mainly found in the following two important scenarios: (i) imposed real-valued angular frequency $\omega$ to determine the complex-valued wavevector $\mathbf{k}$, for the study of wave propagation problems, and (ii) imposed real-valued wavevector $\mathbf{k}$ to determine the complex-valued angular frequency, for the study of time-related problems. We focus here on case (i) and investigate wave propagation in metamaterials as in the left panel of Fig. 2, assuming a real-valued angular frequency. In practice, we fix the direction of propagation along one of the principal axes of the 3D lattice (in the following we assume $\mathbf{k} = k\hat{\mathbf{x}}$) and find numerically, for each angular frequency $\omega$, modes with complex wavenumber propagating inside the periodic array with the electric or magnetic field polarized both in the transverse (along $y$ or $z$) and in the longitudinal (along $x$) directions. We want to stress that the analysis of complex wavenumber is not trivial and only a few studies are devoted to that, such as [23,35,36]. This is a further motivation for our present work. As we will see in the following, the eigenmodes with transverse polarization computed by solving Eqs. (15) and (16) coincide. However, since the electric and magnetic fields are decoupled for longitudinal propagation, these equations give distinct wavenumbers for modes with either the electric or the magnetic field polarized longitudinally.

### E. Dyadic Expressions for Equivalent Parameters

An alternative representation to the four dyadics (12) to describe the electromagnetic properties of the infinite periodic system involves the definition of *equivalent* parameters rather than effective parameters. Equivalent parameters embed the contribution of the out-of-diagonal tensors $\bar{\bar{\boldsymbol{\zeta}}}_{\mathrm{eff}}$ and $\bar{\bar{\boldsymbol{\xi}}}_{\mathrm{eff}}$ into permittivity and permeability, as done in scalar form in [11]. In this way, the four dyadics of Eq. (12) reduce to two *equivalent* dyadics, the equivalent permittivity $\bar{\bar{\varepsilon}}_{\mathrm{eq}}$ and permeability $\bar{\bar{\boldsymbol{\mu}}}_{\mathrm{eq}}$ defined by

$$\mathbf{D}_{\mathrm{av}} = \bar{\bar{\varepsilon}}_{\mathrm{eff}} \cdot \mathbf{E}_{\mathrm{av}} + \bar{\bar{\boldsymbol{\xi}}}_{\mathrm{eff}} \cdot \mathbf{H}_{\mathrm{av}} = \bar{\bar{\varepsilon}}_{\mathrm{eq}} \cdot \mathbf{E}_{\mathrm{av}},$$
$$\mathbf{B}_{\mathrm{av}} = \bar{\bar{\boldsymbol{\mu}}}_{\mathrm{eff}} \cdot \mathbf{H}_{\mathrm{av}} + \bar{\bar{\boldsymbol{\zeta}}}_{\mathrm{eff}} \cdot \mathbf{E}_{\mathrm{av}} = \bar{\bar{\boldsymbol{\mu}}}_{\mathrm{eq}} \cdot \mathbf{H}_{\mathrm{av}}. \quad (17)$$

The transformation of the out-of-diagonal dyadics is again realized with the help of Maxwell equations without sources, which gives Eq. (14) and leads to the expression of the equivalent permittivity and permeability dyadics as

$$\bar{\bar{\varepsilon}}_{\mathrm{eq}}(\omega, \mathbf{k}) = \bar{\bar{\varepsilon}}_{\mathrm{eff}} + \bar{\bar{\boldsymbol{\xi}}}_{\mathrm{eff}} \cdot \bar{\bar{\boldsymbol{\mu}}}_{\mathrm{eff}}^{-1} \cdot \left( \frac{\mathbf{k}}{\omega} \times \bar{\bar{\mathbf{I}}} - \bar{\bar{\boldsymbol{\zeta}}}_{\mathrm{eff}} \right),$$
$$\bar{\bar{\boldsymbol{\mu}}}_{\mathrm{eq}}(\omega, \mathbf{k}) = \bar{\bar{\boldsymbol{\mu}}}_{\mathrm{eff}} - \bar{\bar{\boldsymbol{\zeta}}}_{\mathrm{eff}} \cdot \bar{\bar{\varepsilon}}_{\mathrm{eff}}^{-1} \cdot \left( \frac{\mathbf{k}}{\omega} \times \bar{\bar{\mathbf{I}}} + \bar{\bar{\boldsymbol{\xi}}}_{\mathrm{eff}} \right). \quad (18)$$

As mentioned in [11], equivalent parameters can be used to model the array scattering properties. However, they should not be used to separately describe the electric and magnetic response of a metamaterial as the frequency dispersion of the equivalent parameters may contain nonphysical artifacts and may not satisfy passivity, reciprocity, or other causality constraints typical of local parameters [11,37,38], as will also be shown in the next section.

## 3. ILLUSTRATIVE EXAMPLES FOR A 3D LATTICE OF $TiO_2$ MICROSPHERES IN THE THz RANGE

We apply in this section the formalism introduced in Section 2 to a 3D cubic lattice of $TiO_2$ microspheres of radius $R = 52$ μm embedded in free space ($\varepsilon_h = \varepsilon_0$) with a filling fraction of 29.44% (corresponding to a lattice period $a = 126$ μm). For the chosen microsphere's size, the first dipolar Mie magnetic resonance appears around 300 GHz as illustrated in the right panel of Fig. 2 by the plot of the magnitude of Mie scattering coefficients in Eq. (3). However, note that around 300 GHz residual electric effects due to the electric resonance around 420 GHz are present and need to be considered for accurate results.

We show the result of the eigenmode computation, as well as the $\mathbf{k}$-dependent effective parameters. The effects of magnetoelectric coupling as well as spatial dispersion are emphasized. By comparison with full-wave simulations we confirm the improved accuracy of the method in Section 2 for the modeling of 3D lattices as the ones analyzed in this paper.

### A. Modes with Complex Wavenumber Supported by a 3D Lattice of $TiO_2$ Microspheres

In this section, we show the complex wavenumbers of the modes propagating along the $x$ direction ($\mathbf{k} = k\hat{\mathbf{x}}$), with electric and magnetic fields polarized along the $y$ or $z$ directions and along the $x$ direction. We show only modes whose power flow is toward the positive $x$ direction (i.e., with $\mathrm{Im}(k) > 0$) and restrict ourselves to showing only modes with low or moderate attenuation constant such that $\mathrm{Im}(ka/\pi) < 1.5$.

The trajectories in the complex plane of the complex wavenumbers when frequency is varying, relative to the modes with longitudinal and transverse polarization, are shown for a frequency range between 200 to 500 GHz together with the corresponding wavenumber dispersion diagram for each mode in Fig. 3.

For a normalized attenuation $0 < \mathrm{Im}(ka/\pi) < 1.5$, we find five modes in the structure, two longitudinal and three transverse, as detailed in the following subsections. Since we restrict ourselves to the modes whose power flow is toward the positive $x$ direction, those with $\mathrm{Re}(ka/\pi) > 0$ are forward modes (modes 1 and 2 longitudinal and modes 1 and 3 transverse) and those with $\mathrm{Re}(ka/\pi) < 0$ are backward modes (mode 2 transverse) [28].

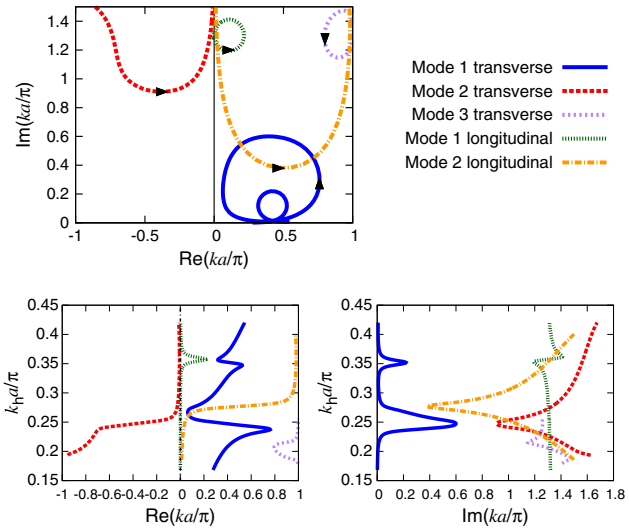


Fig. 3. Top row: trajectories in the complex plane of both longitudinal and transverse normalized wavenumbers computed with Eqs. (15) and (16) for a cubic array of $TiO_2$ microspheres of 52 μm with a filling fraction of 29.44%. Bottom row: dispersion diagrams (real and imaginary parts) corresponding to the wavenumber of each mode.

### 1. Longitudinal Modes

#### a. Mode Characterized by the Electric Field Polarized Along the Direction of Propagation

Mode 1 longitudinal, computed with Eq. (15), exhibits an electric field polarized along the direction of propagation. The real and imaginary parts of the normalized wavenumber pertaining to this mode are shown in Fig. 3 as a function of normalized frequency, which corresponds to a frequency range between 200 and 500 GHz. This longitudinal eigenmode is strongly attenuated and is a static mode in almost the entire frequency range since $\mathrm{Re}(k) = 0$. This behavior confirms the absence of free charges inside the medium, in accordance with the Maxwell equation associated with the divergence of the electric field.

#### b. Mode Characterized by the Magnetic Field Polarized Along the Direction of Propagation

Mode 2 longitudinal, computed with Eq. (16), exhibits a magnetic field polarized along the direction of propagation. Both real and imaginary parts of the normalized wavenumber pertaining to this mode are also shown in Fig. 3. This longitudinal eigenmode is also strongly attenuated, static at low frequency, and experiencing a change of behavior at $(k_h a/\pi) = 0.28$, corresponding to $f = 329$ GHz. This mode exactly corresponds to the longitudinal mode reported previously in [23].

### 2. Transverse Modes and Dominant Mode

Modes 1, 2, and 3 transverse have both electric and magnetic fields orthogonal to the direction of propagation. For the structure at hand, only one transverse polarized mode (mode 1) is dominant; i.e., its imaginary part in the frequency range of interest is smaller than the imaginary part of any other transverse mode, and contributes the most to the field in the array as shown in [14,23]. Modes 2 and 3 are instead largely attenuated and thus evanescent. Mode 1 transverse can then be used to deduce the effective properties of the periodic array giving an accurate description of the physical properties of the structure. In Fig. 3 we can see that mode 1 transverse experiences two resonances at $(k_h a/\pi) = 0.245$ and 0.35 (i.e., $f = 290$ and 415 GHz) that correspond to the first dipolar Mie magnetic and electric resonances of the dielectric microspheres, respectively (see Fig. 2).

## B. Effective Parameters

The effective parameters given by Eq. (12) depend on the pair $(\omega, \mathbf{k})$, where each parameter is in general arbitrary. To have a general understanding of the effect of spatial dispersion on the effective parameters, we compute Eq. (12) for three different real values of the wavevector: $\mathbf{k} = \mathbf{0}$, $\frac{\pi}{2a}\hat{\mathbf{x}}$, $\frac{\pi}{a}\hat{\mathbf{x}}$ for the frequency range 220–380 THz that includes the first magnetic dipolar resonance of the $TiO_2$ microspheres. As a remark, we consider in this section the effect of the wavevector on the effective parameters but, for the sake of clarity, only for real values of $\mathbf{k}$. However, as shown in the previous section, $\mathbf{k}$ is in general complex, and a wider range of effects can be observed (change in the amplitude of resonance, for instance).

We show in Figs. 4 and 5 the $yy$ (same of $zz$) and $xx$ components of both relative permittivity and permeability tensors. We first remark that in Fig. 4 spatial dispersion has a strong influence on the $yy$ component of the effective permittivity since it gives rise to a new (though weak) resonance (the effective permittivity is nearly constant in the absence of spatial dispersion), but affects only weakly its $xx$ component.

On the other hand, the strong magnetic resonance of both $xx$ and $yy$ components of the effective permeability is weakly

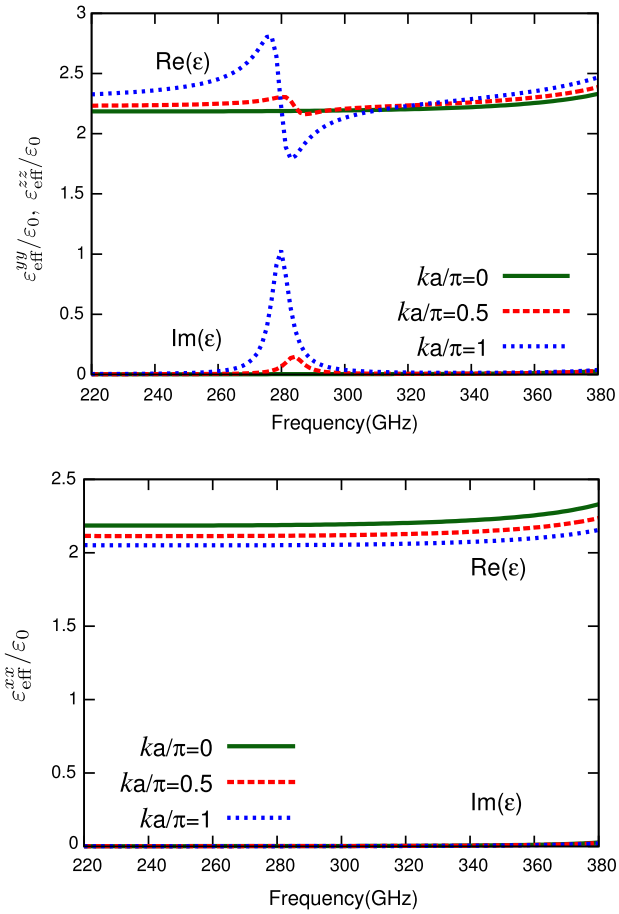


Fig. 4. $yy$, $zz$, and $xx$ components of the relative effective permittivity in Eq. (12) computed for three different values of the wavevector $\mathbf{k} = \mathbf{0}$, $\frac{\pi}{2a}\hat{\mathbf{x}}$, $\frac{\pi}{a}\hat{\mathbf{x}}$.

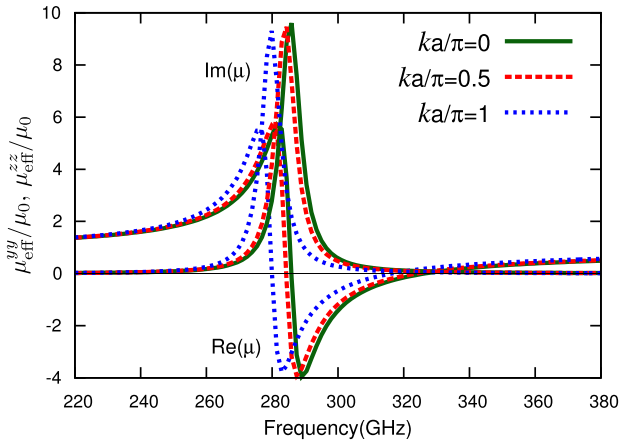


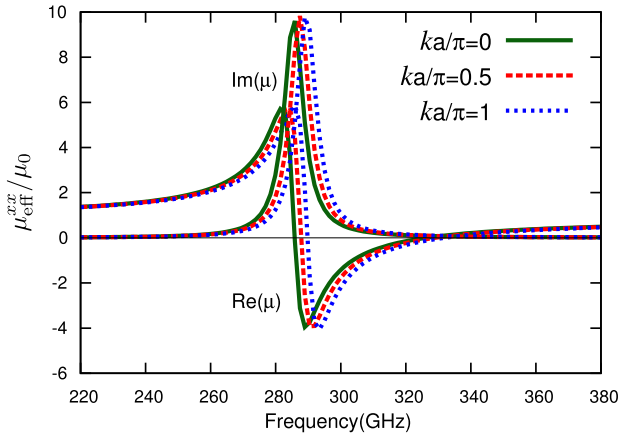


Fig. 5. $yy$, $zz$, and $xx$ components of the relative effective permeability in Eq. (12) computed for three different values of the wavevector $\mathbf{k}=\mathbf{0}$, $\frac{\pi}{2a}\,\hat{\mathbf{x}}$, $\frac{\pi}{a}\,\hat{\mathbf{x}}$.

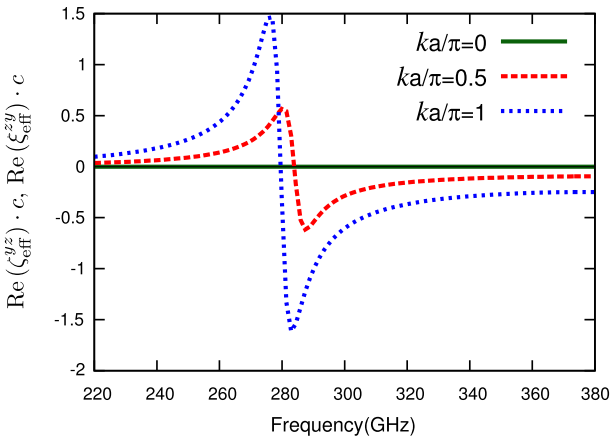


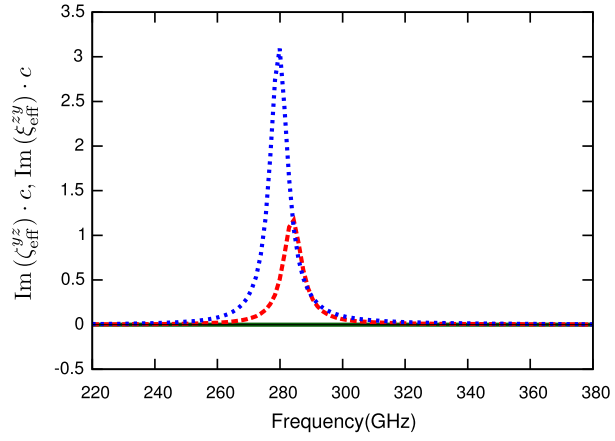


Fig. 6. Main component of the relative out-of-diagonal tensors, normalized by $\sqrt{\epsilon_0\mu_0}=1/c$, computed for three different values of the wavevector $\mathbf{k}=\mathbf{0}$, $\frac{\pi}{2a}\,\hat{\mathbf{x}}$, $\frac{\pi}{a}\,\hat{\mathbf{x}}$.

affected by spatial dispersion as shown in Fig. 5. This collective magnetic Mie dipolar resonance of the array of microspheres is robust with respect to the wavevector.

For a wavevector directed along one of the main axes of the cubic array, in this case the $x$ axis, the out-of-diagonal dyadics $\bar{\bar{\boldsymbol{\zeta}}}_{\rm eff}$ and $\bar{\bar{\boldsymbol{\xi}}}_{\rm eff}$ are of the form

$$\bar{\bar{\boldsymbol{\zeta}}}_{\rm eff}=\begin{bmatrix}0&0&0\\0&0&\zeta_{\rm eff}^{yz}\\0&\zeta_{\rm eff}^{zy}&0\end{bmatrix}\qquad \bar{\bar{\boldsymbol{\xi}}}_{\rm eff}=\begin{bmatrix}0&0&0\\0&0&\xi_{\rm eff}^{yz}\\0&\xi_{\rm eff}^{zy}&0\end{bmatrix},\tag{19}$$

and possess, due to reciprocity, the following properties: $\xi_{\rm eff}^{yz}=-\xi_{\rm eff}^{zy}=\zeta_{\rm eff}^{zy}=-\zeta_{\rm eff}^{yz}$. Thus, only one component of the tensor is needed to describe the electromagnetic coupling, and we plot in Fig. 6 the $yz$ component of the out-of-diagonal tensor $\bar{\bar{\boldsymbol{\xi}}}_{\rm eff}$. It can be noted that the tensors $\bar{\bar{\boldsymbol{\xi}}}_{\rm eff}$ and $\bar{\bar{\boldsymbol{\zeta}}}_{\rm eff}$ are different from zero when spatial dispersion is present but null when $\mathbf{k}=\mathbf{0}$: bianisotropy (due to magnetoelectric coupling) in this centrosymmetric system is not arising from a cross coupling of the unit element as in [39], but as stated in [11], is a direct consequence of weak spatial dispersion associated with the nonzero value of the wavevector [because $\bar{\bar{\mathbf{C}}}_{\rm em}(\mathbf{k}=\mathbf{0})=\bar{\bar{\mathbf{0}}}$].

### C. Scattering Properties: Comparison with Full-Wave Simulations

In this section, we compare the results obtained with the method in Section 2 to the one given by finite-element simulations with HFSS software. We simulate a five-layer slab of a cubic array of $TiO_2$ microspheres, represented in Fig. 7, illuminated by a normally incident plane wave. The cubic array of lattice period $a=126$ μm is five layers long along the direction of propagation and infinite along the other directions.

#### 1. Reflection and Transmission Coefficients

We use the method in Section 2 to calculate the reflection and transmission coefficients from a five-layer slab of $TiO_2$ metamaterial. We assume the slab to be homogenizable with thickness $d=5a$ as in Fig. 7. We use the standard Fresnel formulas [40]

$$S_{11}=\frac{\Gamma(1-e^{2ikd})}{1-\Gamma^2\cdot e^{2ikd}},\qquad S_{21}=\frac{4z}{(1+z)^2}\cdot\frac{e^{ikd}}{1-\Gamma^2\cdot e^{2ikd}}\tag{20}$$

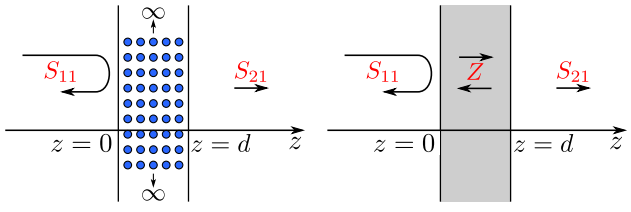


Fig. 7. On the left, representation of the five-layer slab with thickness $d$ of $TiO_2$ microspheres used for HFSS simulations. On the right, equivalent homogeneous slab of same thickness $d$.

where $d$ is the slab thickness, and $k$ is the wavenumber of the dominant mode 1. Moreover, $z$ is the normalized (to free space) characteristic impedance of the metamaterial slab and $\Gamma$ is the single interface reflection coefficient defined by

$$z = \sqrt{\frac{\varepsilon_0 \cdot \mu_{\mathrm{eq}}^{yy}}{\mu_0 \cdot \varepsilon_{\mathrm{eq}}^{yy}}}, \quad \Gamma = \frac{z-1}{z+1}, \tag{21}$$

where $\varepsilon_{\mathrm{eq}}^{yy}$ and $\mu_{\mathrm{eq}}^{yy}$ are the $yy$ components of the equivalent permittivity and permeability tensors (18).

We thus compare in Fig. 8 the magnitude and the phase of reflection and transmission coefficients to the ones obtained directly from HFSS full-wave simulations of a five-layer slab of $TiO_2$ metamaterial. We observe an excellent agreement between the two results that, first, confirms the validity of the dipolar assumption even for high filling fractions. Second, this good agreement also confirms the accuracy of the method in Section 2 (including both spatial dispersion and magnetoelectric coupling) to describe such systems. Third, as we mentioned previously, the equivalent parameters, which reduce the description of the system to two parameters only, give the same scattered field as the original structure (regardless of their physical meaning).

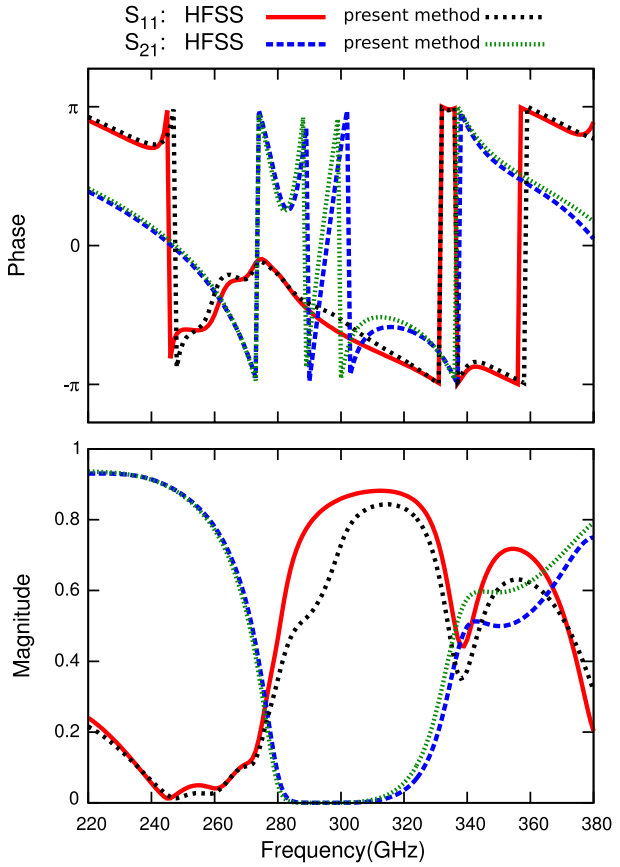


Fig. 8. Comparison between the magnitude and the phase of the $S$ parameters obtained with HFSS and computed with the present method for a cubic array of $TiO_2$ microspheres of 52 μm with a filling fraction of 29.44%.

*2. Equivalent Parameters*

From the $S$ parameters given by the full-wave simulation, it is possible to retrieve the equivalent index and impedance of the simulated material by using the Nicolson–Ross–Weir (NRW) retrieval method [41] (we refer to these parameters as equivalent consistently with the terminology in [11], though they are usually referred to as effective). This method is largely employed in the metamaterial community and is generally used to derive the equivalent permittivity and permeability from the equivalent index and impedance. However, because it assumes that the composite material behaves as a natural material (assumption not always valid for composite materials) an unphysical behavior can be observed [38,41–43].

We compare in Fig. 9 the $yy$ component of the equivalent parameters given by Eq. (18) with the parameters obtained from the full-wave simulation of a five-layer slab with HFSS using the NRW retrieval method [41]. We can see that for both results, the relative permeability experiences a classical resonance behavior, but on the other hand, the relative permittivity experiences an antiresonance in the real part together with a negative imaginary part. This behavior, which violates passivity and causality laws, was justified in [37], where it is claimed that the equivalent parameters, which include the contribution of the out-of-diagonal dyadics $\bar{\bar{\xi}}_{\mathrm{eff}}$ and $\bar{\bar{\xi}}_{\mathrm{eff}}$, as well as the NRW parameters (which assume the metamaterial can be described as a natural material and give nonlocal parameters [7–9]), have no physical meaning for the description of electric and magnetic properties separately [11]. This absence of physical meaning is due to the fact that more complex effects such as magnetoelectric coupling are included inside the permittivity and permeability.

However, by comparing these results, it can be seen that the equivalent permeability agrees very well with full-wave simulations, and more interestingly, the behavior of the permittivity (antiresonance and negative imaginary part) given by the NRW retrieval process is qualitatively reproduced by the present method, and this, only when considering magnetoelectric coupling. As we will see in the next section, the difference of magnitudes between permittivities mainly comes from the disagreement of impedances.

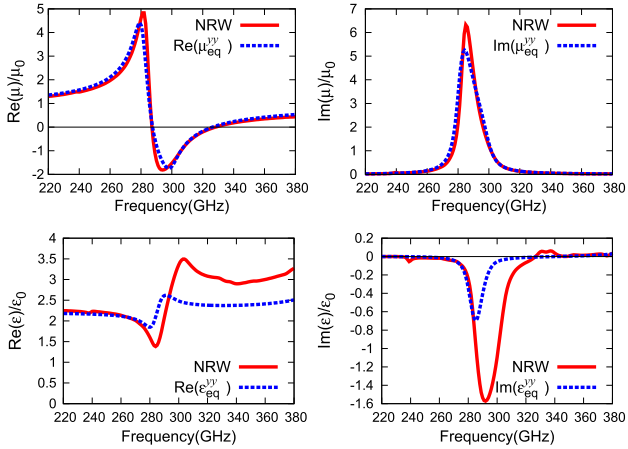


Fig. 9. Comparison between the $yy$ component of the relative equivalent permittivity and permeability (18) and the full-wave relative permittivity and permeability retrieved with NRW method for a cubic array of $TiO_2$ microspheres of 52 μm with a filling fraction of 29.44%.

So, even if these parameters have no physical meaning, they allow us to have physical insight on the underlying mechanism of these noncausal and nonpassive effects already observed in [41–43], i.e., magnetoelectric coupling effects that are forced into permittivity and permeability effects.

### 3. Equivalent Index and Equivalent Impedance

From the dominant complex eigenmode $k$ pertaining to mode 1 transverse in Fig. 3 we can deduce the equivalent refractive index of the composite medium $n_{\mathrm{eq}} = \sqrt{\epsilon_{\mathrm{eq}}^{yy} \cdot \mu_{\mathrm{eq}}^{yy}} = (k/k_0)$.

This index (with or without neglecting the $\bar{\bar{\mathbf{C}}}_{\mathrm{em}}$ dyadic) is compared in Fig. 10 to the one obtained from the full-wave simulation of a five-layer slab with HFSS using the NRW retrieval method. We can see that in this frequency range, the three results agree very well and show a strong resonance associated with the lowest-order Mie dipolar magnetic resonance of the microspheres. However, it is important to note that including the magnetoelectric coupling term $\bar{\bar{\mathbf{C}}}_{\mathrm{em}}$ results in an improved accuracy with respect to the full-wave simulations as already concluded in [39].

Finally, we also compare in Fig. 11 the impedance obtained by full-wave simulations with that computed using the equivalent parameters (21), limiting ourselves to the most accurate case that accounts for $\bar{\bar{\mathbf{C}}}_{\mathrm{em}}$. We observe there exists a disagreement at resonance between the impedances (responsible for the disagreement of the permittivities in Fig. 9). This was previously interpreted in [9] as the difference between surface impedance and Bloch impedance (obtained form numerical simulations) for nonlocal media.

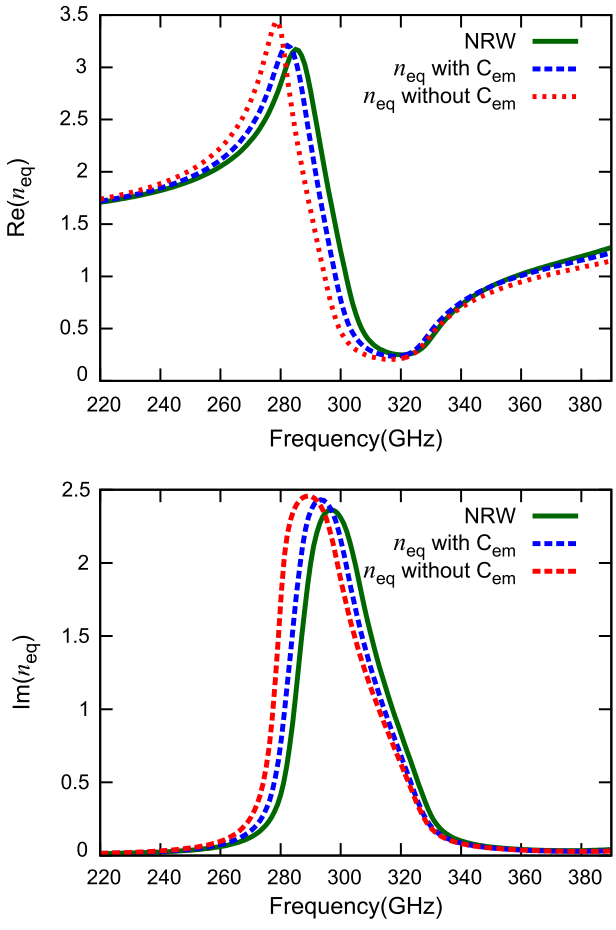


Fig. 10. Comparison between the equivalent refractive index obtained with HFSS (NRW), with the equivalent refractive index computed with the present method taking into account or not the $\bar{\bar{\mathbf{C}}}_{\mathrm{em}}$ dyadic, for a cubic array of $TiO_2$ microspheres of 52 μm with a filling fraction of 29.44%.

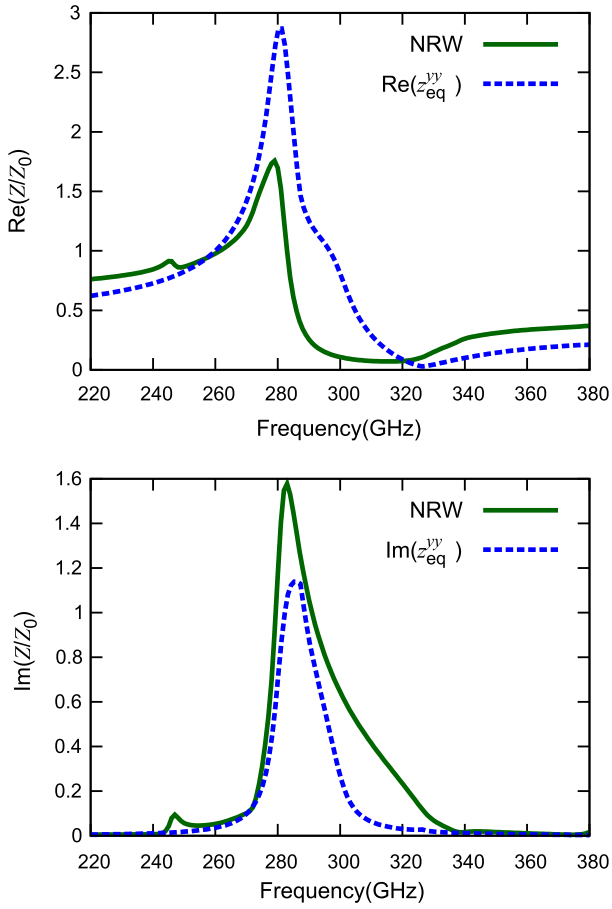


Fig. 11. Comparison between the equivalent relative impedance obtained with HFSS (NRW), with the $yy$ component of the equivalent impedance computed with the present method, for a cubic array of $TiO_2$ microspheres of 52 μm with a filling fraction of 29.44%.

## 4. CONCLUSIONS

In this paper, we have shown the accuracy of the generalized Lorentz–Lorenz method reported in [6] to describe the electromagnetic behavior of metamaterials made of a cubic array of $TiO_2$ microspheres embedded in a host medium around the first Mie magnetic dipolar resonance and under normal illumination. We have observed good agreement with full-wave simulations under the assumption of dipolar approximation (both electric and magnetic, coupled). We have emphasized the effect of the magnetoelectric coupling as well as weak spatial dispersion effects in this kind of systems. Finally, we have confirmed the underlying physical mechanism giving rise to artifacts into the equivalent parameters (antiresonance in the real part and negative imaginary part of the equivalent permittivity) reported in [37]. This effect is observed when one forces the description of the complex electromagnetic behavior (such as spatial dispersion and electromagnetic coupling) into permeability and permittivity contributions, defining the so-called equivalent parameters [11,37].

## ACKNOWLEDGMENTS

The authors acknowledge partial support from the European Science Foundation (ESF) within the framework of the ESF activity "New Frontiers in Millimetre/Sub-Millimetre Waves Integrated Dielectric Focusing Systems" and also from the European Commission 7th Framework Program FP7/2008, "Nanosciences, Nanotechnologies, Materials and New Production Technologies (NMP)" theme, research area "NMP-2008-2.2-2 Nanostructured metamaterials," grant agreement no. 228762. The work by S. C and F. C has been partially supported by the USA National Science Foundation, award NSF-CMMI 1101074.

## REFERENCES

1. S. Tretyakov, *Analytical Modeling in Applied Electromagnetics* (Artech House, 2003).
2. R. E. Collin, *Field Theory of Guided Waves* (IEEE, 1991).
3. A. H. Sihvola, *Electromagnetic Mixing Formulas and Applications* (IET, 1999).
4. J. C. Maxwell-Garnett, "Colours in metal glasses and in metallic films," Philos. Trans. R. Soc. London Ser. A **203**, 385–420 (1904).
5. R. Ruppin, "Evaluation of extended Maxwell–Garnett theories," Opt. Commun. **182**, 273–279 (2000).
6. M. G. Silveirinha, "Generalized Lorentz–Lorenz formulas for microstructured materials," Phys. Rev. B **76**, 245117 (2007).
7. C. R. Simovski and S. A. Tretyakov, "Local constitutive parameters of metamaterials from an effective-medium perspective," Phys. Rev. B **75**, 195111 (2007).
8. C. R. Simovski, "Bloch material parameters of magneto-dielectric metamaterials and the concept of bloch lattices," Metamaterials **1**, 62–80 (2007).
9. C. R. Simovski, "Material parameters of metamaterials (a review)," Opt. Spectrosc. **107**, 726–753 (2009).
10. C. Fietz and G. Shvets, "Current-driven metamaterial homogenization," Physica B **405**, 2930–2934 (2010).
11. A. Alù, "First-principles homogenization theory for periodic metamaterials," Phys. Rev. B **84**, 075153 (2011).
12. S. Campione and F. Capolino, "Ewald method for 3D periodic dyadic Green's functions and complex modes in composite materials made of spherical particles under the dual dipole approximation," Radio Sci. **47**, RS0N06 (2012).
13. X. Liu and A. Alu, "Generalized retrieval method for metamaterial constitutive parameters based on a physically driven homogenization approach," Phys. Rev. B **87**, 235136 (2013).
14. S. Campione, M. Sinclair, and F. Capolino, "Effective medium representation and complex modes in 3d periodic metamaterials made of cubic resonators with large permittivity at mid-infrared frequencies," Photon. Nanostr. Fundam. Appl. **11**, 423–435 (2013).
15. O. Vendik and M. Gashinova, "Artificial double negative (DNG) media composed by two different dielectric sphere lattices embedded in a dielectric matrix," in *34th European Microwave Conference*, Vol. **3** (IEEE, 2005), pp. 1209–1212.
16. L. Jylhä, I. Kolmakov, S. Maslovski, and S. Tretyakov, "Modeling of isotropic backward-wave materials composed of resonant spheres," J. Appl. Phys. **99**, 043102 (2006).
17. V. Yannopapas and A. Moroz, "Negative refractive index metamaterials from inherently non-magnetic materials for deep infrared to terahertz frequency ranges," J. Phys. Condens. Matter **17**, 3717–3734 (2005).
18. M. Wheeler, J. Aitchison, and M. Mojahedi, "Three-dimensional array of dielectric spheres with an isotropic negative permeability at infrared frequencies," Phys. Rev. B **72**, 193103 (2005).
19. I. Vendik, M. Odit, and D. Kozlov, "3D isotropic metamaterial based on a regular array of resonant dielectric spherical inclusions," Metamaterials **3**, 140–147 (2009).
20. S. Lannebre, "Étude théorique de métamatériaux formés de particules diélectriques résonantes dans la gamme submillimétrique: magnétisme artificiel et indice de réfraction négatif," Ph.D. thesis (Université Bordeaux, 2011).
21. K. Berdel, J. Rivas, P. Bolivar, P. de Maagt, and H. Kurz, "Temperature dependence of the permittivity and loss tangent of high-permittivity materials at terahertz frequencies," IEEE Trans. Microw. Theor. Tech. **53**, 1266–1271 (2005).
22. N. Matsumoto, T. Hosokura, K. Kageyama, H. Takagi, Y. Sakabe, and M. Hangyo, "Analysis of dielectric response of $TiO_2$ in terahertz frequency region by general harmonic oscillator model," Jpn. J. Appl. Phys. **47**, 7725–7728 (2008).
23. S. Campione, S. Lannebère, A. Aradian, M. Albani, and F. Capolino, "Complex modes and artificial magnetism in three-dimensional periodic arrays of titanium dioxide microspheres at millimeter waves," J. Opt. Soc. Am. B **29**, 1697–1706 (2012).
24. S. Steshenko and F. Capolino, *Metamaterials Handbook: Applications of Metamaterials* (CRC, 2009), Chap. 8.
25. G. Mulholland, C. Bohren, and K. Fuller, "Light scattering by agglomerates—coupled electric and magnetic dipole method," Langmuir **10**, 2533–2546 (1994).
26. C. Bohren and D. Huffman, *Absorption and Scattering of Light by Small Particles* (Wiley-Interscience, 1983).
27. M. Abramowitz and I. A. Stegun, *Handbook of Mathematical Functions with Formulas, Graphs, and Mathematical Tables* (Dover, 1964).
28. S. Campione, S. Steshenko, M. Albani, and F. Capolino, "Complex modes and effective refractive index in 3d periodic arrays of plasmonic nanospheres," Opt. Express **19**, 26027–26043 (2011).
29. G. Lovat, P. Burghignoli, and R. Araneo, "Efficient evaluation of the 3-D periodic Green's function through the Ewald method," IEEE Trans. Microw. Theor. Tech. **56**, 2069–2075 (2008).
30. I. Stevanovic and J. Mosig, "Periodic Green's function for skewed 3-D lattices using the Ewald transformation," Microw. Opt. Technol. Lett. **49**, 1353–1357 (2007).
31. A. Alù and N. Engheta, "Polarizabilities and effective parameters for collections of spherical nanoparticles formed by pairs of concentric double-negative, single-negative, and/or double-positive metamaterial layers," J. Appl. Phys. **97**, 094310 (2005).
32. J. A. Kong, *Electromagnetic Wave Theory* (Wiley-Interscience, 1990).
33. I. V. Lindell, A. Sihvola, S. A. Tretyakov, and A. J. Viitanen, *Electromagnetic Waves in Chiral and Bi-Isotropic Media* (Artech House, 1994).
34. M. G. Silveirinha, "Metamaterial homogenization approach with application to the characterization of microstructured composites with negative parameters," Phys. Rev. B **75**, 115104 (2007).
35. R. A. Shore and A. D. Yaghjian, "Complex waves on periodic arrays of lossy and lossless permeable spheres: 1. Theory," Radio Sci. **47**, RS2014 (2012).
36. R. A. Shore and A. D. Yaghjian, "Complex waves on periodic arrays of lossy and lossless permeable spheres: 2. Numerical results," Radio Sci. **47**, RS2015 (2012).
37. A. Alù, "Restoring the physical meaning of metamaterial constitutive parameters," Phys. Rev. B **83**, 081102 (2011).
38. P. Alitalo, A. Culhaoglu, C. Simovski, and S. Tretyakov, "Experimental study of anti-resonant behavior of material parameters in periodic and aperiodic composite materials," J. Appl. Phys. **113**, 224903 (2013).
39. R. Marqus, F. Medina, and R. Rafii-El-Idrissi, "Role of bianisotropy in negative permeability and left-handed metamaterials," Phys. Rev. B **65**, 144440 (2002).
40. J. A. Stratton, *Electromagnetic Theory* (McGraw-Hill, 1941).
41. D. R. Smith, S. Schultz, P. Markoš, and C. M. Soukoulis, "Determination of effective permittivity and permeability of metamaterials from reflection and transmission coefficients," Phys. Rev. B **65**, 195104 (2002).
42. T. Koschny, P. Markoš, D. R. Smith, and C. M. Soukoulis, "Resonant and antiresonant frequency dependence of the effective parameters of metamaterials," Phys. Rev. E **68**, 065602 (2003).
43. D. R. Smith, D. C. Vier, T. Koschny, and C. M. Soukoulis, "Electromagnetic parameter retrieval from inhomogeneous metamaterials," Phys. Rev. E **71**, 036617 (2005).